Tensor factorizations of local second-order Møller–Plesset theory

Jun Yang' , Yuki Kurashige' , Frederick R. Manby' , and Garnet K. L. Chan'

Tensor factorizations of local second-order Møller–Plesset theory

Jun Yang,[1,a)] Yuki Kurashige,[2,b)] Frederick R. Manby,[3,c)] and Garnet K. L. Chan[4,d)]

[1]*Department of Chemistry and Chemical Biology, Cornell University, Ithaca, New York 14853, USA*
[2]*Department of Theoretical and Computational Molecular Science, Institute for Molecular Science, 38 Nishigo-Naka, Myodaiji, Okazaki 444-8585, Japan*
[3]*Center for Computational Chemistry, School of Chemistry, University of Bristol, Bristol BS8 1TS, United Kingdom*
[4]*Department of Chemistry and Chemical Biology, Cornell University, Ithaca, New York 14853, USA*

Efficient electronic structure methods can be built around efficient tensor representations of the wavefunction. Here we first describe a general view of tensor factorization for the compact representation of electronic wavefunctions. Next, we use this language to construct a low-complexity representation of the doubles amplitudes in local second-order Møller–Plesset perturbation theory. We introduce two approximations—the direct orbital-specific virtual approximation and the full orbital-specific virtual approximation. In these approximations, each occupied orbital is associated with a small set of correlating virtual orbitals. Conceptually, the representation lies between the projected atomic orbital representation in Pulay–Saebø local correlation theories and pair natural orbital correlation theories. We have tested the orbital-specific virtual approximations on a variety of systems and properties including total energies, reaction energies, and potential energy curves. Compared to the Pulay–Saebø ansatz, we find that these approximations exhibit favorable accuracy and computational times while yielding smooth potential energy curves. © *2011 American Institute of Physics*. [doi:10.1063/1.3528935]

I. INTRODUCTION

In electron correlation there are two problems of complexity. The first relates to the information (storage) required to represent the wavefunction and the second to the complexity of manipulating the wavefunction to calculate observables. Consider, for example, the doubles amplitudes t_{ij}^{ab} (where ij denote occupied orbitals, ab denote virtual orbitals) common to the second-order Møller–Plesset perturbation (MP2), coupled cluster doubles (CCD), and coupled electron pair approximations (CEPA). The storage scales like N^4 while the cost of obtaining the energy scales like N^5 for MP2 and N^6 for CCD and CEPA, where N is a measure of the size of the system.

In several limits, we expect these formal complexities to be too high. For example, if there is a large number of atomic orbitals on a single center, there is redundancy in the product occupied-virtual pair basis. Also, in large molecules the cost to obtain the energy should be linear in the size of the molecule. In both these situations, the mismatch between formal complexity and our expected complexity suggests that the amplitudes and amplitude equations have some special structure. For example, in Pulay–Saebø local correlation theories based on the projected atomic orbital (PAO) ansatz,[1–3] the sparsity structure of the amplitudes is built in through distance-based truncations,[4] and using this framework it has been possible to achieve linear scaling of storage and computational cost with system size.[5–9] Naturally, these trunca-

tions are not orbitally invariant and require a representation of the orbitals in which the amplitude matrix is maximally sparse. An important task in devising algorithms with reduced complexities is to find optimal transformations of the amplitudes to representations that are approximable with low complexity.

The doubles amplitude t_{ij}^{ab} is a tensorial quantity. Here, by tensor we do not refer to the transformation properties (as used, for example, in nonorthogonal representations,[10,11]), but simply to the fact that many indices are involved. The problem of finding a low-complexity representation can be viewed as one of tensor representations or tensor factorizations. While there has been much recent work in constructing low-complexity representations for the doubles amplitudes and two-electron integrals, both through using more optimal orbitals (for example, along the lines of local pair natural orbitals (LPNOs) (Refs. 10 and 12–17), optimized virtual orbital spaces,[18,19] frozen natural orbitals,[20–23] and others[24,25]) as well as matrix factorizations of the integrals and amplitudes (such as Cholesky decompositions and density fitting (DF) (or resolutions of the identity, RI) (Refs. 26–36), these approaches have not yet explored the full generality of the tensorial structure.

The current work has two goals. The first is to establish language with which we can discuss tensor factorization in a general way. In particular, this will allow us to classify different tensor factorizations by the topology and nature of their connectivities. The second goal is to explore a specific factorization which we refer to as an orbital-specific virtual approximation. This representation has a simple and intuitive interpretation that bridges earlier work on optimal virtuals and work on PNOs. We explore the orbital-specific virtual

a)Electronic mail: jy459@cornell.edu.
b)Electronic mail: kura@ims.ac.jp.
c)Electronic mail: fred.manby@bris.ac.uk.
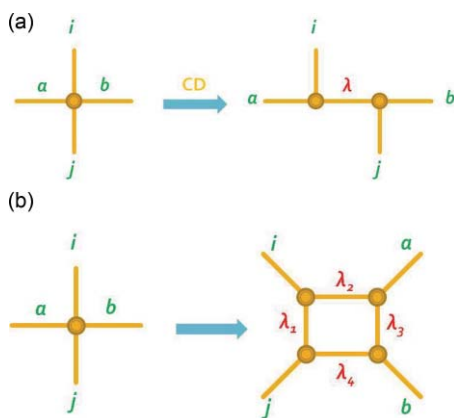d)Electronic mail: gc238@cornell.edu.

FIG. 1. Pictorial representations of (a) Cholesky decomposition and (b) matrix product decomposition.

approximation in the context of local second-order Møller–Plesset perturbation theory. We present applications on a variety of large molecules, clusters, and reactions. We find that the ansatz is very favorable both in its formal properties such as potential energy curve smoothness, and weak computational dependence on the size of the underlying basis, as well as regarding its absolute costs in terms of storage and timings when compared to an existing efficient implementation of the local Pulay–Saebø correlation ansatz.[6,37] Finally, we finish with a discussion of the future prospects of such an approach.

(Note: After this work was completed, we have become aware that Pulay and co-workers have been pursuing an approach for local correlation that is similar to the orbital-specific virtual approximation investigated here.)

II. THEORY AND ALGORITHM

A. Classification of tensor factorizations

We are concerned primarily with the doubles amplitude tensor t_{ij}^{ab}. We illustrate it pictorially as a connected four-point object (see objects on the left in Figs. 1 and 2). A closely related quantity, particularly in second-order Møller–Plesset theory, is the two-electron integral v_{ij}^{ab}. In canonical closed-shell MP2 theory, the two are related by

$$t_{ij}^{ab} = \left(2v_{ij}^{ab} - v_{ij}^{ba}\right)\left(\epsilon_i + \epsilon_j - \epsilon_a - \epsilon_b\right)^{-1}. \tag{1}$$

To construct a low-complexity representation of the two-electron integrals or amplitudes, we approximate the high-dimensional amplitude or integral tensors by lower-dimensional components. These component tensors may share the same "physical" indices i, j, a, b as the target tensor, but may also carry additional "auxiliary" indices $\lambda, \mu, \nu, \rho, \ldots$. Since the auxiliary indices do not appear in the target tensor, they must be traced over in some way, and both the distribution of the physical and auxiliary indices among the component tensors as well as the pattern of contractions define the particular tensor representation. Since these contractions are usually nonlinear, it is often useful to visualize the contractions pictorially rather than algebraically.

To illustrate this, consider first the density-fitting and Cholesky decomposition approximations. In all these approximations, the two-electron integrals are viewed as a matrix factorization,

$$v_{ij}^{ab} = \sum_\lambda L_{i\lambda}^a L_{j\lambda}^b, \tag{2}$$

where λ is the auxiliary index. Pictorially, we view the above as separating the ia, jb electron–hole degrees of freedom, which must then be reconnected via an auxiliary index [see Fig. 1(a)]. Naturally, the efficiency of the factorization relies on the rank of the decomposition (the number of terms in the sum) being low. As another example, consider the types of correlation ansatz (such as the Pulay–Saebø local correlation ansatz) which use a noncanonical virtual orbital basis, for example, the PAO virtuals. Noncanonical virtuals ϕ_μ are related to canonical virtuals ϕ_a by a transformation

$$\phi_\mu = \sum_\mu t_\mu^a \phi_a, \tag{3}$$

and, consequently, the canonical and noncanonical doubles amplitudes are related by

$$t_{ij}^{ab} = \sum_{\mu\nu} t_{ij}^{\mu\nu} t_\mu^a t_\nu^b, \tag{4}$$

which defines the amplitude approximation. Pictorially, this approximation is illustrated in Fig. 2(a). For appropriate t_μ^a (such as defined by the PAO virtuals), representation (4) allows one to favorably exploit locality. For example, in

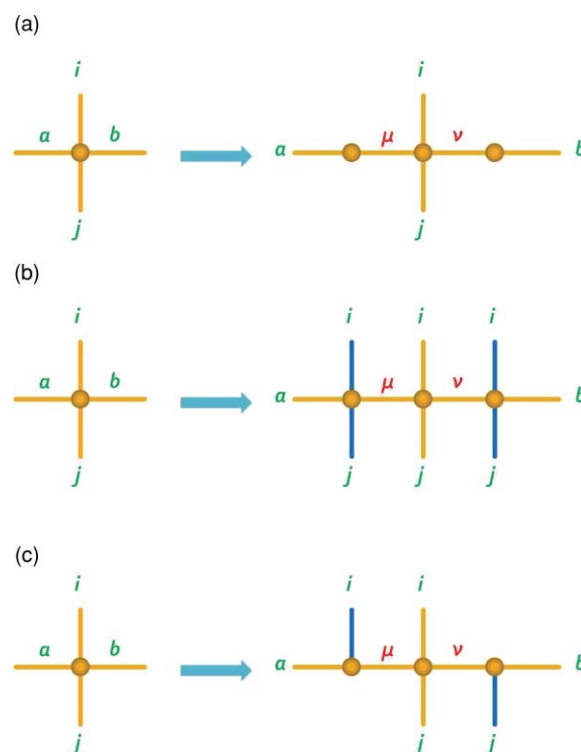FIG. 2. Pictorial representations of (a) $t_{ij}^{ab} = \sum_{\mu\nu} t_{ij}^{\mu\nu} t_\mu^a t_\nu^b$ (Pulay–Saebø PAO approximation), (b) $t_{ij}^{ab} = \sum_{\mu\nu} t_{ija}^{\mu ij} t_{ij}^{\mu_i \nu_j} t_{ijb}^{\nu ij}$ (pair natural orbital approximation), and (c) $t_{ij}^{ab} = \sum_{\mu\nu} t_{ia}^{\mu_i} t_{ij}^{\mu_i \nu_j} t_{jb}^{\nu_j}$ (orbital-specific virtual approximation).

the Pulay–Saebø–Werner–Schütz approaches[1–3,6–9], a sparsity structure on $t_{ij}^{\mu\nu}$ is imposed by requiring $t_{ij}^{\mu\nu} = 0$ when i is far apart from j, and for other ij, the sum over μ and ν is restricted to defined domains $[ij]$ that are in the spatial vicinity of ij.

Thus, the essence of low-complexity tensor approximation is captured by the types of indices on the components and their connectivity, as illustrated in their pictorial representation. We can consider generalizations of the above approximations in a variety of ways. For example, we can consider approximations with additional auxiliary indices. One example is [cf. Fig. 1(b)]

$$t_{ij}^{ab} = \sum_{\lambda_1\ldots\lambda_4} t_i^{\lambda_1\lambda_2} t_{\lambda_2\lambda_3}^a t_{\lambda_3\lambda_4}^b t_j^{\lambda_4\lambda_1} \tag{5}$$

$$= \mathrm{tr}[\mathbf{t}_i \mathbf{t}^a \mathbf{t}^b \mathbf{t}_j] \tag{6}$$

where the amplitude t_{ij}^{ab} is reconstructed as a trace of a matrix product. This approximation recalls the matrix product decomposition in the density matrix renormalization group (DMRG) (Refs. 38 and 39), although the physical content here is quite distinct, since the DMRG is carried out in the occupation number space rather than in the excitation space. Another way to construct new approximations is to introduce components with repeated physical indices. A particularly simple example is

$$t_{ij}^{ab} = t_{ij} t_{ia} t_{jb}, \tag{7}$$

where there are no auxiliary indices at all. This recalls the correlator product state approximation (also known as an entangled plaquette state,[40,41]), although once again the tensor is expressed in an excitation rather than occupation number picture. Naturally, we can consider many other combinations of auxiliary indices and physical indices, and the appropriateness of the particular choice depends on the problem at hand.

B. Orbital-specific virtual approximation

We now consider a simple tensor factorization of the doubles amplitudes t_{ij}^{ab} that we will study in this work. We first define the *direct orbital-specific virtual* (dOSV) approximation to the amplitudes as [cf. Fig. 2(c)]

$$t_{ij}^{ab} = \sum_{\mu\nu} t_{ia}^{\mu_i} t_{ij}^{\mu_i\nu_j} t_{jb}^{\nu_j}. \tag{8}$$

This has a simple physical interpretation: the component $t_{ia}^{\mu_i}$ (and similarly $t_{jb}^{\nu_j}$) defines a set of virtual orbitals for *each* occupied orbital and $t_{ij}^{\mu_i\nu_j}$ represents amplitudes in this orbital-specific basis. Note that the subscript i in μ_i is somewhat redundant, but we retain it to emphasize that μ_i labels an orbital-specific virtual associated with occupied orbital i. By choosing a good set of components $t_{ia}^{\mu_i}$, either by direct optimization or otherwise (see later), we may define suitable adaptations of the virtual basis for each occupied orbital. This is quite natural in a local correlation theory, as the optimal orbital-specific virtuals for a localized occupied orbital must

be located in close spatial proximity; however, even when the occupied orbitals are delocalized, we can still expect this factorization to be beneficial, as a given occupied orbital does not correlate equally with all parts of the virtual space.

In the dOSV approximation, occupied orbital i excites only to its virtual set μ_i ($i \to \mu_i$) and occupied orbital j only to its orbital set ν_j ($j \to \nu_j$): the "exchange" excitations $i \to \nu_j$, $j \to \mu_i$ being excluded. It was shown, however, in the context of Pulay–Saebø local theory that the inclusion of exchange excitations can lead to greatly improved results.[42–45] While formally the exchange excitations can be included by increasing the size of sets μ_i and ν_j, we can also include them explicitly in the structure of the ansatz, which leads to the full orbital-specific virtual (OSV) approximation

$$t_{ij}^{ab} = \sum_{\mu\nu} \Big(t_{ia}^{\mu_i} t_{ij}^{\mu_i\nu_i} t_{jb}^{\nu_i} + t_{ia}^{\mu_i} t_{ij}^{\mu_i\nu_j} t_{jb}^{\nu_j}$$
$$+ t_{ia}^{\mu_j} t_{ij}^{\mu_j\nu_i} t_{jb}^{\nu_i} + t_{ia}^{\mu_j} t_{ij}^{\mu_j\nu_j} t_{jb}^{\nu_j} \Big). \tag{9}$$

This can be written in matrix form

$$t_{ij}^{ab} = \sum_{\mu\nu} \begin{pmatrix} t_{ia}^{\mu_i} & t_{ia}^{\mu_j} \end{pmatrix} \begin{pmatrix} t_{ij}^{\mu_i\nu_i} & t_{ij}^{\mu_i\nu_j} \\ t_{ij}^{\mu_j\nu_i} & t_{ij}^{\mu_j\nu_j} \end{pmatrix} \begin{pmatrix} t_{jb}^{\nu_i} \\ t_{jb}^{\nu_j} \end{pmatrix}. \tag{10}$$

To gain further understanding, we briefly discuss the connection to other approximations where noncanonical virtual spaces are used. In theories which use a global set of noncanonical virtuals, such as the PAO virtual space in the Pulay–Saebø ansatz, the amplitude tensor is expressible as in Eq. (4), where t_μ^a and t_ν^b parametrize the transformation to a new virtual basis. In PNO theories pioneered some time ago[10,12–15] and which have been recently revisited by Neese and co-workers,[16,17] a correlating virtual space is defined for each occupied pair ij, and the amplitudes are factorized as (cf. Fig. 2(b))

$$t_{ij}^{ab} = \sum_{\mu\nu} t_{ija}^{\mu_{ij}} t_{ij}^{\mu_i\nu_j} t_{ijb}^{\nu_{ij}}. \tag{11}$$

Compared to the Pulay–Saebø ansatz where a global set of virtuals is used, the orbital-specific virtual approximation is able to adapt the virtual space, which leads to a more compact representation of the amplitudes. On the other hand, the orbital-specific virtual approximation adapts each virtual space to a single occupied orbital rather than a pair. This avoids some of the complexities inherent to the PNO ansatz where the definitions of the virtual spaces involve four-index components $t_{ija}^{\mu_{ij}}$ of similar formal complexity to the amplitudes themselves and which lead to virtual blocks of overlap and Fock matrices with higher dimensions (e.g., $S_{\mu_{ij}\nu_{kl}}$) in the PNO space than those in the orbital-specific virtual space (e.g., $S_{\mu_i\nu_k}$). Consequently, we see that formally the orbital-specific virtual approximation interpolates between the Pulay–Saebø form and the PNO approximation. We now turn toward its practical implementation in second-order perturbation theory (MP2).

III. IMPLEMENTATION

A. MP2 wavefunction and singular value orbital-specific virtuals

The central task of MP2 theory is to determine the first-order wavefunction $|\Psi^{(1)}\rangle$,

$$|\Psi^{(1)}\rangle = \frac{1}{2}\sum_{ijab} t_{ij}^{ab}|\Phi_{ij}^{ab}\rangle \qquad (12)$$

where in the above $i, j, \ldots$ and $a, b, \ldots$ refer, respectively, to the occupied and virtual *spatial* orbitals. Explicitly in spin-orbital notation

$$|\Phi_{ij}^{ab}\rangle = \sum_{\sigma,\sigma'\in\{\alpha,\beta\}} |\Phi_{i\sigma j\sigma'}^{a\sigma b\sigma'}\rangle. \qquad (13)$$

For closed-shell molecules the spin-free orbital notation avoids the explicit use of spin coordinates and is very convenient.

Inserting the orbital-specific virtual approximation [cf. Eq. (8)] into Eq. (12), we parametrize the first-order wavefunction in terms of factorized amplitudes $t_{ij}^{\mu_i\nu_j}$ and corresponding determinants $|\Phi_{ij}^{\mu_i\nu_j}\rangle$. For the direct orbital-specific virtual approximation of Møller–Plesset perturbation (dOSVMP2),

$$|\Psi^{(1)}\rangle = \frac{1}{2}\sum_{ij\mu\nu} t_{ij}^{\mu_i\nu_j}|\Phi_{ij}^{\mu_i\nu_j}\rangle, \qquad (14)$$

where

$$|\Phi_{ij}^{\mu_i\nu_j}\rangle = \sum_{ab} t_{ia}^{\mu_i}|\Phi_{ij}^{ab}\rangle t_{jb}^{\nu_j}, \qquad (15)$$

while for the full orbital-specific virtual approximation of Møller–Plesset perturbation (OSVMP2), we have

$$|\Psi^{(1)}\rangle = \frac{1}{2}\sum_{ij\mu\nu}\Big(t_{ij}^{\mu_i\nu_i}|\Phi_{ij}^{\mu_i\nu_i}\rangle + t_{ij}^{\mu_i\nu_j}|\Phi_{ij}^{\mu_i\nu_j}\rangle + t_{ij}^{\mu_j\nu_i}|\Phi_{ij}^{\mu_j\nu_i}\rangle$$
$$+ t_{ij}^{\mu_j\nu_j}|\Phi_{ij}^{\mu_j\nu_j}\rangle\Big). \qquad (16)$$

In Eq. (14) we have introduced an orbital-specific virtual $|\mu_i\rangle$ defined through an orbital transformation from the virtual $|a\rangle$ using $t_{ia}^{\mu_i}$,

$$|\mu_i\rangle = \sum_a t_{ia}^{\mu_i}|a\rangle. \qquad (17)$$

Naturally, we would like the OSVs to be well adapted to each occupied orbital in Eq. (17). One quick and economical scheme to determine $t_{ia}^{\mu_i}$ is to perform a singular value decomposition (SVD) of the MP2 diagonal amplitudes t_{ii}^{ab} for *each* occupied orbital i,

$$t_{ii}^{ab} = \sum_\mu t_{ia}^{\mu_i} s_{\mu_i} t_{ib}^{\mu_i}, \qquad (18)$$

where s_{μ_i} is the singular value. In the canonical basis, t_{ii}^{ab} is directly calculated from

$$t_{ii}^{ab} = \frac{v_{ii}^{ab}}{2\epsilon_i - \epsilon_a - \epsilon_b}. \qquad (19)$$

When the localized occupied orbitals are used, ϵ_i is the diagonal element of the Fock matrix in the local orbital basis. ϵ_a and ϵ_b are the diagonal elements of the virtual block of Fock matrix.

The SVD provides a natural setting to truncate the OSV space, as the singular vectors with small singular values s_μ should contribute little to the final amplitudes. Consequently it is reasonable to include only those vectors with the largest eigenvalues, keeping either a fixed number of OSVs per occupied orbital, a fixed percentage of OSVs, or by using a numerical threshold on s_μ. We have used the first two truncation schemes in this work. After truncation, the complete virtual space is parametrized by an incomplete set of orbital-specific virtuals. This, of course, introduces errors relative to canonical MP2 theory. However, as numerically shown in Sec. IV, the resulting correlation energies exhibit only minor deviations (e.g., $< 0.01\%$) from canonical values while achieving very substantial gains in computational efficiency.

The OSVs defined above are not always orthogonal. The overlap matrix between the OSVs $|\mu_i\rangle$ and $|\nu_j\rangle$ is

$$S_{\mu_i\nu_j} = \langle\mu_i|\nu_j\rangle = \sum_a t_{ia}^{\mu_i} t_{ja}^{\nu_j}. \qquad (20)$$

Through the SVD, the OSVs $|\mu_i\rangle$ belonging to the same occupied orbital are orthonormal but the OSVs from different occupied orbitals are not.

We also note that the SVD does not necessarily yield the most optimal orbital-specific virtual orbitals. The optimization of $t_{ia}^{\mu_i}$ relaxes the OSVs and may help achieve a more compact description of the correlation effects. This is under investigation and will be presented elsewhere.

B. Residual equations

We derive the exact MP2 residual equations in the OSV basis starting from the Hylleraas functional,[46]

$$h = \langle\Psi^{(1)}|F - E^{(0)}|\Psi^{(1)}\rangle + 2\langle\Psi^{(1)}|V|\Psi^{(0)}\rangle, \qquad (21)$$

where F is the Fock operator and V is the two-electron fluctuation potential. $E^{(0)}$ is the sum of occupied Hartree–Fock eigenvalues. By parametrizing $\Psi^{(1)}$ in the dOSVMP2 [cf. Eq. (14)] and making the first derivative of h with respect to $t_{ij}^{\mu_i\nu_j}$ vanish, we arrive at the following formal residual,

$$R_{ij}^{\mu_i\nu_j} = \left(\frac{\partial h}{\partial t_{ij}^{\mu_i\nu_j}}\right) = \langle\Phi_{ij}^{\mu_i\nu_j}|F - E^{(0)}|\Psi^{(1)}\rangle$$
$$+ \langle\Phi_{ij}^{\mu_i\nu_j}|V|\Psi^{(0)}\rangle = 0. \qquad (22)$$

The expansion of $R_{ij}^{\mu_i\nu_j}$ has the following explicit form for a particular pair (i, j),

$$R_{(i,j)} = 2K_{(i,j)} - J_{(i,j)} + 2\Big[T_{(i,j)}F_{(j,j)} + F_{(i,i)}T_{(i,j)}$$
$$- \sum_k F_{kj}T_{(i,k)}S_{(k,j)} - \sum_k F_{ik}S_{(i,k)}T_{(k,j)}\Big]$$
$$- S_{(i,j)}\Big[T_{(j,i)}F_{(j,j)} - \sum_k F_{ik}T_{(j,k)}S_{(k,j)}\Big]$$
$$- \Big[F_{(i,j)}T_{(j,i)} - \sum_k F_{kj}S_{(i,k)}T_{(k,i)}\Big]S_{(i,j)}. \qquad (23)$$

Here $T_{(i,j)}$ is the matrix form of amplitudes $\{t_{ij}^{\mu_i \nu_j}\}$, fixing i, j. F_{ik} and F_{kj} are elements of the occupied block of the Fock matrix. $K_{(i,j)}$ and $J_{(i,j)}$ denote the matrices storing two-electron exchange and Coulomb integrals $(\phi_i \phi_{\mu_i} | \phi_j \phi_{\nu_j})$ and $(\phi_i \phi_{\nu_j} | \phi_j \phi_{\mu_i})$, respectively. $S_{(i,j)}$ and $F_{(i,j)}$ are, respectively, the overlap and Fock matrices with elements $\langle \phi_{\mu_i} | \phi_{\nu_j} \rangle$ and $\langle \phi_{\mu_i} | \hat{F} | \phi_{\nu_j} \rangle$ for a pair (i, j). None of the above quantities give rise to real bottlenecks for memory or disk storage if the orbital-specific virtual space is truncated.

In the OSVMP2 [cf. Eq. (16)], we minimize the Hylleraas functional with respect to the amplitudes $t_{ij}^{\mu_i \nu_i}$, $t_{ij}^{\mu_i \nu_j}$, $t_{ij}^{\mu_j \nu_i}$, $t_{ij}^{\mu_j \nu_j}$ giving rise to analogs of Eq. (22). The explicit residuals are then

$$R_{(i,j)} = K_{(i,j)} + \sum_k \{ S_{(ij,ik)} T_{(i,k)} [\delta_{kj} F_{(ik,ij)} - F_{kj} S_{(ik,ij)}]$$
$$+ [\delta_{ik} F_{(ij,kj)} - F_{ik} S_{(ij,kj)}] T_{kj} S_{(kj,ij)} \}, \qquad (24)$$

where $R_{(i,j)}$ is now a matrix of dimension $\dim(\mu_i) + \dim(\nu_j)$, with elements of types $R_{ij}^{\mu_i \nu_i}$, $R_{ij}^{\mu_i \nu_j}$, $R_{ij}^{\mu_j \nu_i}$, $R_{ij}^{\mu_j \nu_j}$, and similar to $K_{(i,j)}$. $S_{(ij,ik)}$ is the overlap matrix assembled between the bras $\{ \langle \mu_i |, \langle \mu_j | \}$ and the kets $\{ |\nu_i\rangle, |\nu_k\rangle \}$ once needed,

$$S_{(ij,ik)} = \begin{bmatrix} S_{(i,i)} & S_{(i,k)} \\ S_{(j,i)} & S_{(j,k)} \end{bmatrix}, \qquad (25)$$

and $F_{(ij,ik)}$ is the analogously defined Fock matrix.

C. Projective residual equations for dOSVMP2 (dOSVMP2-P)

Compared to the standard local MP2 residual equations, those for the orbital-specific virtuals appear more complicated, especially for the direct (dOSVMP2) ansatz. Formally, we can obtain the MP2 amplitudes not only through variational minimization of the Hylleraas functional but also by projection with an appropriate set of bra states. In the case of dOSVMP2, this leads to a simpler set of residual equations which define a different set of amplitudes than those arising from Eq. (23). We write

$$\widetilde{R}_{ij}^{\mu_i \nu_j} = \langle \widetilde{\Phi}_{ij}^{\mu_i \nu_j} | F - E^{(0)} | \Psi^{(1)} \rangle + \langle \widetilde{\Phi}_{ij}^{\mu_i \nu_j} | V | \Psi^{(0)} \rangle = 0. \quad (26)$$

The bra states are chosen to be biorthonormal to the ket states in the spatial orbital basis following Refs. 2 and 47,

$$\langle \widetilde{\Phi}_{ij}^{\mu_i \nu_j} | \Phi_{kl}^{\omega_k \gamma_l} \rangle = \frac{1}{\sqrt{1 + \delta_{ij}\delta_{\mu_i \nu_j}}} (\delta_{ik}\delta_{jl}\delta_{\mu\omega}\delta_{\nu\gamma} + \delta_{jk}\delta_{il}\delta_{\nu\omega}\delta_{\mu\gamma})$$

$$(27)$$

with a normalization prefactor. The biorthonormal OSV bra state $\langle \widetilde{\Phi}_{ij}^{\mu_i \nu_j} |$ is defined from the canonical biorthonormal bra state $\langle \widetilde{\Phi}_{ij}^{ab} |$,

$$\langle \widetilde{\Phi}_{ij}^{\mu_i \nu_j} | = \sum_{ab} \langle \widetilde{\Phi}_{ij}^{ab} | t_{ia}^{\mu_i} t_{jb}^{\nu_j}, \qquad (28)$$

with[47]

$$\langle \widetilde{\Phi}_{ij}^{ab} | = \tfrac{1}{3}(2\langle \Phi_{ij}^{ab} | + \langle \Phi_{ij}^{ba} |),$$

$$\langle \widetilde{\Phi}_{ij}^{ab} | \Phi_{kl}^{cd} \rangle = \frac{1}{\sqrt{1 + \delta_{ij}\delta_{ab}}} (\delta_{ik}\delta_{jl}\delta_{ac}\delta_{bd} + \delta_{jk}\delta_{il}\delta_{bc}\delta_{ad}).$$

$$(29)$$

Note that if we truncate the OSV space, then the space spanned by the bras $\{ \langle \tilde{\Phi}_{ij}^{\mu_i \nu_j} | \}$ is not the same as the space spanned by $\{ \langle \Phi_{ij}^{\mu_i \nu_j} | \}$ due to the presence of the exchange-like excitation $\langle \Phi_{ij}^{ba} |$ in the definition of $\langle \tilde{\Phi}_{ij}^{ba} |$. This is what gives rise to the difference between the projective and (standard) Hylleraas based residual equations for the dOSVMP2 approximation.

Thus expanding Eq. (26) yields the projective residual equation $\widetilde{R}_{(i,j)}$,

$$\widetilde{R}_{(i,j)} = K_{(i,j)} + \widetilde{T}_{(i,j)} F_{(j,j)} + F_{(i,i)} \widetilde{T}_{(i,j)} - \sum_k F_{kj} \widetilde{T}_{(i,k)} S_{(k,j)}$$
$$- \sum_k F_{ik} S_{(i,k)} \widetilde{T}_{(k,j)}, \qquad (30)$$

which has clearly a simpler form than the standard residual in Eq. (23). We denote the direct orbital-specific virtual approximation defined by the amplitudes from Eq. (30), the projective dOSVMP2-P approximation. In a complete virtual space, the solution of either dOSVMP2 or dOSVMP2-P yields the exact canonical MP2 energy and the first-order wavefunction. In an incomplete virtual space (e.g., if not all the orbital-specific virtuals are used), however, dOSVMP2-P generally does not result in a correlation energy that is variationally bounded above the canonical MP2 value with respect to the size of incomplete virtual space. The numerical comparison between dOSVMP2 and dOSVMP2-P will be given in Sec. IV.

D. Preconditioning

As the Fock matrix is diagonal in the canonical basis, the canonical MP2 amplitudes are directly calculated as

$$t_{ij}^{ab} = \frac{v_{ij}^{ab}}{\epsilon_i + \epsilon_j - \epsilon_a - \epsilon_b}, \qquad (31)$$

where ϵ's are the diagonal elements of the canonical Fock matrix. However, in the orbital-specific virtual space, the Fock matrix contains significant off-diagonal elements and the residual equations must be solved iteratively. Here the use of a preconditioner is essential. To this end we define pseudovirtual energies. The pseudovirtual energies can be obtained by diagonalizing the Fock matrix in the space of orbital-specific virtuals for each diagonal occupied pair (i,i) similar to as done in Ref. 5,

$$F_{(i,i)} X_{(i,i)} = S_{(i,i)} X_{(i,i)} \overline{E}_{(i,i)}, \qquad (32)$$

where $X_{(i,i)}$ is the transformation matrix that diagonalizes both $F_{(i,i)}$ and $S_{(i,i)}$. $\overline{E}_{(i,i)}$ is diagonal and contains the pseudovirtual energies. When preconditioning the residual $R_{(i,j)}$

corresponding to orbital pair (i, j), we then consider the residual as a matrix with the first index corresponding to the virtuals associated with i and the second with the virtuals associated with j. Consequently, the transformation is performed on the virtual indices of the original residual $R_{(i,j)}$ with $X^\dagger_{(i,i)}$ and $X_{(j,j)}$, respectively.

$$\overline{R}_{(i,j)} = X^\dagger_{(i,i)} R_{(i,j)} X_{(j,j)}. \qquad (33)$$

The amplitude update matrix $\Delta\bar{t}_{(i,j)}$ in the transformed basis is then

$$\Delta\bar{t}^{\mu_i \nu_j}_{ij} = \frac{\overline{R}^{\mu_i \nu_j}_{ij}}{\epsilon_i + \epsilon_j - \overline{\epsilon}_{\mu_i} - \overline{\epsilon}_{\nu_j}}, \qquad (34)$$

where $\overline{R}^{\mu_i \nu_j}_{ij}$ is the element of the residual matrix $\overline{R}_{(i,j)}$. The pseudovirtual energies of $\overline{\epsilon}_{\mu_i}$ and $\overline{\epsilon}_{\nu_j}$ are the elements of $\overline{E}_{(i,i)}$ and $\overline{E}_{(j,j)}$, respectively. Finally the update in the original orbital-specific basis is given by the back-transformation

$$\Delta t_{(i,j)} = X_{(i,i)} \Delta\bar{t}_{(i,j)} X^\dagger_{(j,j)}. \qquad (35)$$

The same algorithm can be used with both dOSVMP2 and OSVMP2, the latter requiring the obvious generalizations of indices (i, j) to (i, i), (i, j), (j, i), (j, j).

Note that for OSVMP2 the eigenvectors $X_{(i,j)}$ may be linearly dependent. (The same issue arises, e.g., in the Pulay–Saebø local correlation theory[5]). The redundant vectors are eliminated by a canonical orthogonalization of $S_{(i,j)}$, discarding eigenvalues of $S_{(i,j)}$ below a given linear dependency threshold (not to be confused with the screening threshold T_S later). Here we use a linear dependency threshold of 10^{-6} for all OSVMP2 calculations.

With the above preconditioning, the amplitudes and MP2 energies converge very quickly. For example, typically, the change in correlation energy falls below 10^{-6} a.u. within 8–10 iterations for dOSVMP2-P and OSVMP2 and within 16–20 iterations for dOSVMP2.

E. Computational cost and screening

The most expensive term in our current implementation of the residual equations (23) and (30) is the contraction $\sum_k F_{kj} T_{(i,k)} S_{(k,j)}$, similar to the corresponding terms in the local Pulay–Saebø ansatz. In the Pulay–Saebø ansatz this term can be computed in two ways, i.e., the contractions can be carried out inside or outside the summation but both lead to O^3 scalings in large molecules if we use all occupied pairs.[6] In the case of OSV approaches for large molecules, the contraction also scales as O^3 though we expect (and find in our numerical results below) that the prefactor of the O^3 term is better than that of the PAO implementation due to the smaller number of OSVs needed for a given accuracy.

We can further lower the computational cost by introducing some screening approximations to the N^6 contraction. As we have discussed previously, the most important OSVs that can be correlated with each occupied orbital are located close to the occupied orbital itself. By exploiting orbital locality, the overlap matrix element $S_{\gamma_k \nu_j}$ decays exponentially with the separation of k and j. Based on this we can simply ignore

entire classes of unimportant N^6 contractions in the residuals without losing much accuracy and consequently reduce the scaling of solving the residual equations in a large system to order O^2. The following ratio t^S_{kj} for a given pair (k, j) is computed in order to define an appropriate screening threshold,

$$t^S_{kj} = \frac{\sum_{\gamma \nu} S^2_{\gamma_k \nu_j}}{\sum_{\gamma \nu} S^2_{\gamma_k \nu_k}}. \qquad (36)$$

With a screening threshold of T_S we then neglect any overlap matrix $S_{(k,j)}$ belonging to a pair (k, j) if $t^S_{kj} < T_S$. From the definition, t^S_{kj} ranges between 0 and 1: thus when $T_S = 0$ the overlap matrices belonging to all pairs of (k, j) are taken into account; when $T_S = 1$ only the diagonal contributions with $k = j$ are included. Equation (36) allows us to avoid a less desirable spatial truncation criterion.

Currently, however, the main cost in our OSVMP2 implementation is the integral transformation, since the full local occupied space is employed throughout transforming complete two-electron integrals. For example, without using sparsity, the first-quarter integral transformation $(\alpha\beta|\gamma\delta) \to (i\beta|\gamma\delta)$ scales as N^5 and limits the size of molecules that we can treat efficiently. As has been previously demonstrated by Werner and co-workers,[5,6] however, a linear scaling transformation algorithm can be achieved by discarding spatially distant occupied orbital pairs and exploiting integral prescreening techniques. DF/RI techniques in local approximations[35,36] can further decrease the cost of integral transformations by 1–2 orders of magnitude for large molecules. These techniques will be incorporated into our algorithm in future work.

IV. COMPARING THE dOSVMP2 AND OSVMP2 APPROXIMATIONS

We have introduced two related factorizations of MP2 theory, dOSVMP2 and OSVMP2. In addition, in dOSVMP2 we can define the amplitudes through two different residual equations: one obtained via the Hylleraas functional (dOSVMP2), and one obtained by projection (dOSVMP2-P). These variants have been implemented in the quantum chemistry program DALTON.[48] We now assess the numerical behavior of these different schemes for correlation energies and reaction energies. All calculations were performed with $T_S = 0$ unless the T_S is explicitly given. The internal orbitals were localized using Boys localization[49] throughout the present work.

A. Correlation energies

The number of OSVs associated with each occupied orbital [the number of μ_i or ν_i in, e.g., Eq. (8)] needed to recover a given accuracy in the correlation energy relative to the canonical MP2 energy is reported for polyglycine oligopeptides, water clusters, and polyene chains. As seen in Table I, a small number of OSVs recover most of the correlation energy (e.g., $\geq 99.5\%$); the precise number depends on the electronic structure of the molecule. OSVMP2 (which includes the exchange excitations) requires far fewer OSVs to reach the same

TABLE I. Comparisons of the number of OSVs needed to obtain different accuracies (99.5%, 99.9%, and 99.99%) in the MP2 correlation energies using dOSVMP2, dOSVMP2-P, and OSVMP2 approximations, respectively. The cc-pVDZ basis sets (Ref. 50) were used. The canonical MP2 reference correlation energies were obtained using the MOLPRO program package (Ref. 37). N_v is the total number of canonical virtual orbitals. The cartesian coordinates of $[gly]_n$ and $(H_2O)_n$ are given in Refs. 51 and 52, respectively.

$[gly]_n$		dOSVMP2			dOSVMP2-P			OSVMP2		
n	N_v	99.5%	99.9%	99.99%	99.5%	99.9%	99.99%	99.5%	99.9%	99.99%
1	75	35	51	65	32	48	63	16	22	31
2	131	41	62	91	38	58	88	18	25	39
4	243	44	68	103	42	65	99	19	28	44
6	355	46	70	106	43	66	103	19	28	46
8	467	46	71	108	43	67	103	19	28	46
12	691	47	71	108	44	68	104	20	29	46
14	803	47	72	109	44	68	105	20	29	47
$(H_2O)_n$		dOSVMP2			dOSVMP2-P			OSVMP2		
n	N_v	99.5%	99.9%	99.99%	99.5%	99.9%	99.99%	99.5%	99.9%	99.99%
10_{prism}	190	24	35	62	23	33	59	13	17	25
12_{Pr444}	228	24	37	71	24	35	66	13	18	27
14_{Pr2444}	266	24	37	71	24	35	66	13	18	28
16_{Pr4444}	304	25	38	75	24	36	70	13	18	28
$18_{Pr44244}$	342	25	38	75	24	36	70	13	18	28
$19_{globular}$	361	25	39	78	24	36	73	13	18	29

accuracy than dOSVMP2, typically less than half. Nonetheless both approximations are very compact. The number of OSVs to reach a given accuracy also becomes independent of the total molecular size very rapidly. For OSVMP2 the correlation energy is saturated at accuracies of 99.5%, 99.9%, and 99.99%, respectively, with 20, 29, and 47 orbitals for $[gly]_n$ and with 13, 18, and 29 orbitals for $(H_2O)_n$. Note that this saturation behavior is expected when the system size becomes much larger than its correlation length.

Regarding the different residual equations for dOSVMP2 factorization, both yield very similar results. Using the Hylleraas residual (dOSVMP2), we need a few more OSVs than the projected residual (dOSVMP2-P) to recover the same accuracy in the correlation energy. For example, 109 and 105 OSVs, respectively, yield 99.99% accuracy in the correlation energy for dOSVMP2 and dOSVMP2-P for the largest peptide $[gly]_{14}$; for the $(H_2O)_{19}$ cluster we require 78 and 73 OSVs to reach the same accuracy.

Compared to $[gly]_n$ and $(H_2O)_n$, the polyene molecule exhibits significant electronic delocalization, and this leads to longer correlation lengths and more extended orbitals. As a result, it is more difficult to converge the correlation en-

ergy toward the canonical limit than that in other molecules. For example, with 40 OSVs the OSVMP2 error increases from 0.46% to 0.66% (cf. Table II) as the length of polyene chain increases from C_6H_8 to $C_{14}H_{16}$. Note that this decrease in accuracy is physical and not a failure of extensivity of the theory: as the HOMO (highest occupied molecular orbital)–LUMO (lowest unoccupied molecular orbital) gap of the polyenes decreases with increasing chain length, the correlation length increases.

B. Reaction energies

Relative energies are the central quantity in chemistry rather than absolute energies. We have investigated their accuracy by computing relative energies for some isomerization reactions using the different orbital-specific virtual approximations. These reactions were selected from Ref. 53 for the good agreement between the canonical MP2 isomerization energies with triple-ζ basis sets [cc-pVTZ (Ref. 50)] and the experimental isomerization energies. Results for other reactions from the ISO34 test set are given in the supplementary material.[51] The results of dOSVMP2-P and OSVMP2

TABLE II. Comparison of the relative errors of dOSVMP2, dOSVMP2-P, and OSVMP2 correlation energies for polyenes using different numbers of virtual orbitals (40, 80, 100, and 140). cc-pVTZ basis sets were used. The canonical MP2 reference correlation energies were obtained using the MOLPRO program package (Ref. 37). N_v is the total number of canonical virtual orbitals. The cartesian coordinates of polyenes are given in Ref. 51.

Polyenes	N_v	dOSVMP2			dOSVMP2-P			OSVMP2	
		80 (%)	100 (%)	140 (%)	80 (%)	100 (%)	140 (%)	40 (%)	80 (%)
C_6H_8	270	0.80	0.39	0.10	0.67	0.31	0.07	0.46	0.02
C_8H_{10}	351	0.99	0.52	0.17	0.85	0.42	0.13	0.54	0.03
$C_{10}H_{12}$	432	1.12	0.61	0.22	0.97	0.51	0.17	0.59	0.03
$C_{12}H_{14}$	513	1.21	0.68	0.26	1.06	0.57	0.21	0.63	0.03
$C_{14}H_{16}$	594	1.29	0.73	0.29	1.12	0.62	0.23	0.66	0.04

TABLE III. Calculated canonical MP2, dOSVMP2-P, and OSVMP2 isomerization reaction energies (kcal/mol). The dOSVMP2-P and OSVMP2 results are given in the first and second rows for each reaction. The errors given in the parentheses are the deviations relative to canonical MP2 reaction energies. The Ahlrichs-TZV (Refs. 54, 55) basis sets augmented by the cc-pVTZ polarization functions (2d1f, 2p1d) (Ref. 50) were used based on the frozen-core approximation. The fraction (%) of the orbital-specific virtual space used in the calculation is indicated in the first row of the table. The reactions and corresponding molecular geometries were taken from Ref. 53.

Reactions	MP2	10%	20%	40%	60%
7	9.26	10.75 (1.49)	11.10 (1.84)	10.06 (0.80)	9.46 (0.20)
		10.54 (1.28)	9.76 (0.50)	9.28 (0.02)	9.26 (0.00)
8	22.20	20.63 (−1.57)	21.30 (−0.90)	21.82 (−0.38)	22.10 (−0.10)
		21.29 (−0.91)	22.00 (−0.20)	22.19 (−0.01)	22.20 (0.00)
9	6.96	5.17 (−1.79)	5.74 (−1.22)	6.92 (−0.04)	6.94 (−0.02)
		6.54 (−0.42)	6.91 (−0.05)	6.96 (0.00)	6.96 (0.00)
12	47.13	37.61 (−9.52)	47.25 (0.12)	47.01 (−0.12)	47.09 (−0.04)
		45.76 (−1.37)	47.03 (−0.10)	47.12 (−0.01)	47.12 (0.00)
18	11.52	10.75 (−0.77)	11.13 (−0.39)	11.53 (0.01)	11.52 (0.00)
		11.28 (−0.24)	11.48 (−0.04)	11.52 (0.00)	11.52 (0.00)
21	1.08	1.27 (0.19)	1.03 (−0.05)	1.11 (0.03)	1.07 (−0.01)
		1.15 (−0.07)	1.09 (0.01)	1.08 (0.00)	1.08 (0.00)
24	12.56	13.44 (0.88)	12.85 (0.29)	12.36 (−0.20)	12.48 (−0.08)
		12.68 (0.12)	12.52 (−0.04)	12.56 (0.00)	12.56 (0.00)
28	31.12	33.90 (2.78)	33.10 (1.98)	31.74 (0.62)	31.32 (0.20)
		32.64 (1.52)	31.45 (0.33)	31.14 (0.02)	31.12 (0.00)
32	7.35	3.04 (−4.31)	5.70 (−1.65)	7.01 (−0.34)	7.29 (−0.06)
		6.20 (−1.15)	7.15 (−0.20)	7.35 (0.00)	7.35 (0.00)
34	6.98	7.00 (0.02)	5.52 (−1.46)	6.71 (−0.27)	6.97 (−0.01)
		6.62 (−0.36)	6.96 (−0.02)	6.98 (0.00)	6.98 (0.00)
Mean absolute deviations	(kcal/mol)	2.33	0.99	0.28	0.07
		0.74	0.15	0.01	0.00
mean deviations	(kcal/mol)	−1.26	−0.14	0.01	0.01
		−0.15	0.02	0.00	0.00
maximum deviations	(kcal/mol)	9.52	1.98	0.80	0.20
		1.52	0.50	0.02	0.00

computations as well as their deviations from the canonical MP2 values are presented in Table III. The dOSVMP2-P computation using only 10% of the OSVs gives a mean absolute deviation (MAD) of 2.33 kcal/mol. Using 20% of the OSVs drops the MAD to 0.99 kcal/mol. The MAD is further reduced to 0.07 kcal/mol (almost 2 orders of magnitude) when 60% of the OSVs are used.
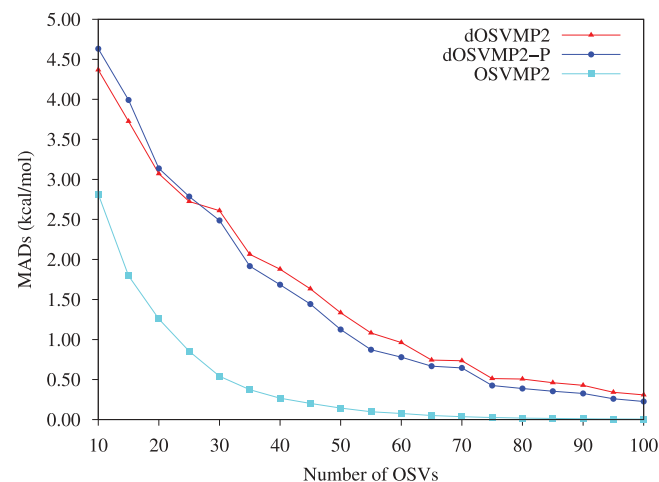

FIG. 3. MADs of the isomerization energies as a function of the number of OSVs using dOSVMP2, dOSVMP2-P, and OSVMP2. The MADs are relative to the canonical MP2 values using the same basis sets.

The MADs of isomerization energies are plotted against the numbers of OSVs per occupied orbital in Fig. 3 for OSVMP2, dOSVMP2-P, and dOSVMP2 schemes. Both dOSVMP2-P and dOSVMP2 display similar accuracies. However, the complete OSVMP2 gives errors that are substantially smaller, and, additionally, these errors decay more rapidly and more smoothly than those of dOSVMP2 and dOSVMP2-P as the number of OSVs used is increased. Nonetheless all methods show a rapid decrease in error as the size of the OSV space is increased.

C. Basis set dependence

We have investigated the orbital-specific virtual orbital dependence of different basis sets using the dOSVMP2-P and OSVMP2 approaches. From previous discussions based on Tables I–III, we expect that the dOSVMP2 model should display a similar basis set dependence compared to dOSVMP2-P. For brevity reasons those results will not be presented here. We have chosen to use a single glycine molecule so that computations with very large basis sets are affordable. As can be seen from Fig. 4, the size of the OSV space (required for a given accuracy in the correlation energy) increases much more slowly than the size of the underlying basis. Moving from cc-pVDZ to cc-pV5Z,[50] the size of the required OSV space for dOSVMP2-P and OSVMP2 increases by a factor of 4–5 while the size of the canonical virtual space increases
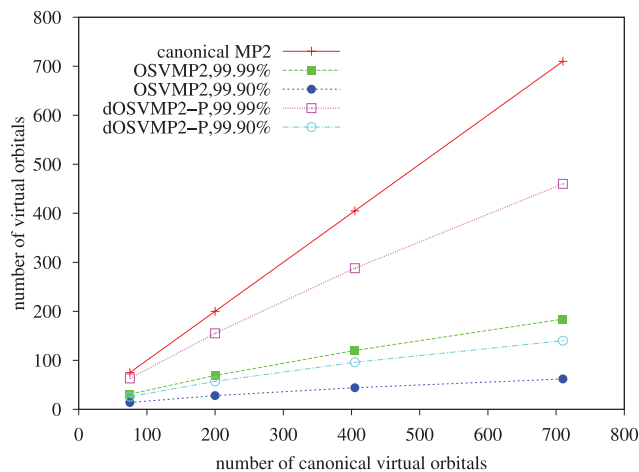
FIG. 4. The number of orbital-specific and canonical virtual orbitals using different basis sets (cc-pVXZ, X = D, T, Q, and 5) for a single glycine molecule. Comparison is made between canonical MP2 (+), dOSVMP2-P (unfilled), and OSVMP2 (filled) for accuracies of 99.90% (circle) and 99.99% (square) of the correlation energy.

almost by a factor of 10. In fact the size of the OSV space needed for a given accuracy appears to increase *sublinearly* with the size of the underlying basis. For example, by using the fitting form $f(x) = a + bx^c$, the power exponents c which characterize the sublinearities are 0.739 (OSVMP2) and 0.808 (dOSVMP2-P) for 99.99% accuracy in the correlation energy and 0.554 (OSVMP2) and 0.617 (dOSVMP2-P) for 99.90% accuracy in the correlation energy. Note that OSVMP2 contains the exchange excitations while the dOSVMP2-P does not. Consequently, the number of virtual orbitals per occupied orbital needed for OSVMP2 is significantly smaller than dOSVMP2-P, roughly half.

D. Visualizing the orbital-specific virtual orbitals

We have visualized the Boys-localized occupied orbitals[49] and a few associated OSVs for a single glycine

molecule in Table IV. These local occupied HOMO, HOMO-4, and HOMO-8 orbitals are chosen to be, respectively, around the N–lone-pair electrons, C–N, and C–C bonds along the skeleton of glycine. Along each column of Table IV, each individual OSV exhibits a different shape for different occupied orbitals. This can be essentially understood from the definition of the OSVs [cf. Eq. (17)] since each OSV has to be adjusted to a particular occupied orbital. For example, the LUMO+4 associated to HOMO, HOMO-4, and HOMO-8 demonstrates, respectively, orbital locality around the N-lone-pair, C–N and C–C bonds, where the associating occupied orbitals are found.

V. COMPARISON WITH THE PULAY–SAEBØ LOCAL MP2 THEORY

The Pulay–Saebø local PAO correlation scheme is a standard against which to compare new approaches to local correlation, such as the orbital-specific virtual approximations used here, we assess both the accuracy and times of the OSVMP2 and dOSVMP2 approximations relative to the Werner–Schütz formulation of the Pulay–Saebø local MP2 as implemented in MOLPRO.[6,37] In the following discussions, the size of OSV virtual space is measured as the number of OSV orbitals per occupied orbital since each OSV orbital is determined for a single occupied orbital rather than for a pair. We note that using the same number of OSVs the whole doubles excitation space in the OSVMP2 model is almost as twice large as that in the dOSVMP2 and dOSVMP2-P models due to the excitations crossing two distinct occupied orbitals [cf. Eq. (10)].

A. Potential energy surfaces

Pulay–Saebø local correlation relies on spatial truncation of virtual orbital domains. Discontinuities on potential energy surfaces (PESs) can then arise since the virtual orbital domain size defined by spatial truncation is not uniform as the geometry is varied. One prototypical example is

TABLE IV. Contour plots of a few Boys-localized occupied orbitals (HOMO, HOMO-4, and HOMO-8) and associated OSVs (LUMO, LUMO + 4, and LUMO + 5) for an isolated single glycine molecule. The cc-pVDZ basis sets were used (Ref. 50). The OSVs are sorted in descending order according to the singular values [cf. Eq. (18)]. HOMO and LUMO correspond to the orbitals, respectively, that have the highest occupied orbital energy and the largest singular value. HOMO-4 and HOMO-8 give the fourth and eighth localized occupied orbitals with orbital energies below the HOMO. LUMO + 4 and LUMO + 5 are the fourth and fifth OSVs with the singular values below the LUMO. The singular values of the selected virtual orbitals are (0.0494, 0.00768, 0.00774) for HOMO, (0.0582, 0.00924 and 0.00878) for HOMO-4, and (0.0555, 0.0108, 0.0094) for HOMO-8.
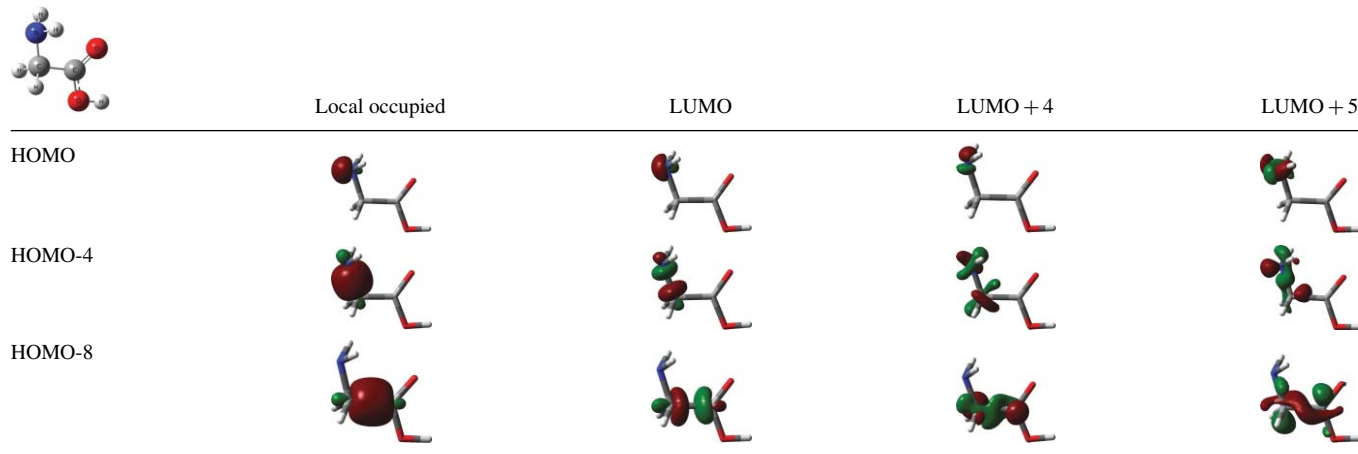
the propadienone (CH_2CCO) molecule that has been recently investigated by Russ and Crawford[56] using local CCSD (coupled cluster singles and doubles) and MP2. Multiple discontinuities occur in the stretching of the central C=C bond of propadienone, even in the vicinity of the equilibrium geometry. The LPNO-CEPA method has been found to give the smoothness of the C–C bond dissociation PES of ketene CH_2CO.[16] Several other attempts have also been made to recover smooth PES in Pulay–Saebø theory. By tailoring and fixing virtual domains,[45] the Pulay–Saebø local approach can avoid these discontinuities. Explicitly correlated R12/F12 methods[57] reduce the magnitude of discontinuities through the auxiliary excitation space.[58,59] There have also been efforts to use bump functions to smooth discontinuous amplitudes.[60] We now reinvestigate this issue using the orbital-specific virtual approximations. We believe that the approach presented here provides a more basic solution.
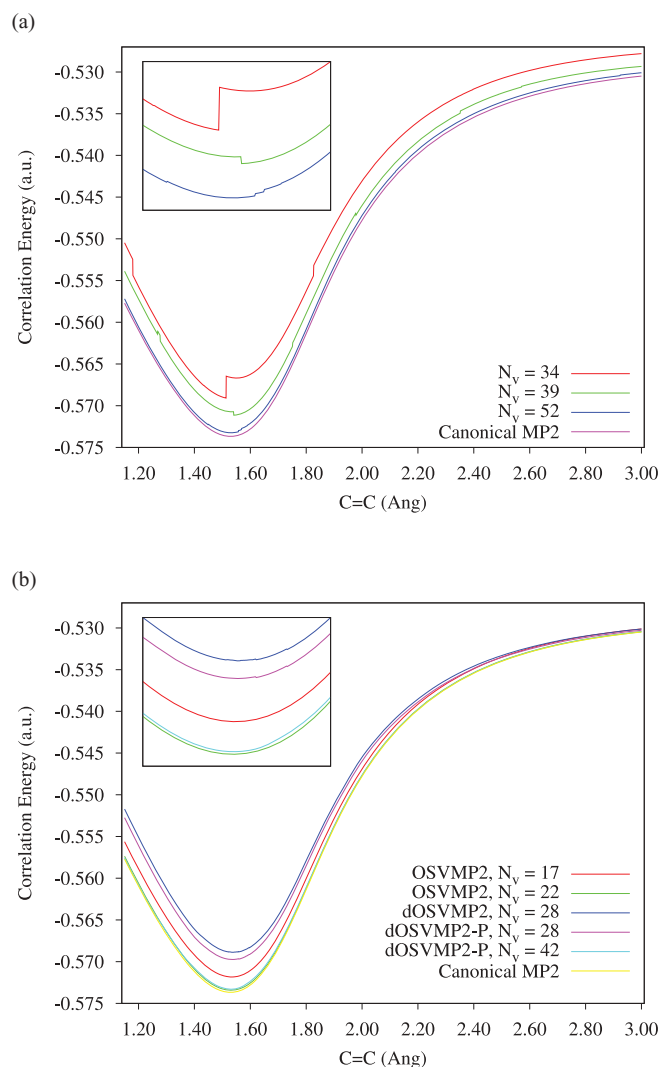
The correlation energy PESs using different numbers of virtual orbitals (N_v) are presented in Fig. 5 for Pulay–Saebø PAO MP2, dOSVMP2, dOSVMP2-P, and OSVMP2. All computations were carried out using the cc-pVDZ basis set[50] with 52 canonical virtual orbitals. For PAO local MP2, N_v denotes the average size of the pair virtual domain. It can be seen that the PES of the PAO based local MP2 with $N_v = 34$ orbitals exhibits three major energy discontinuities in the regions of both short and long C=C bonds as well as around the equilibrium C=C bond. When using $N_v = 39$ PAOs, five smaller discontinuities in the PAO local MP2 theory appear, ranging from 0.2 to 0.4 mE_h at 1.269, 1.540, 1.752, 1.978, and 2.352 Å. A tiny zigzag structure can still be seen in the vicinity of the equilibrium C=C bond even when using $N_v = 52$ PAOs [see inset of Fig. 5(a)].

As for the PES using the orbital-specific virtual approximations, all the dOSVMP2, dOSVMP2-P, and OSVMP2 based curves are smooth even when using much smaller spaces of virtual orbitals. The PES of OSVMP2 displays no discernible discontinuities when using 17 OSVs [cf. Fig. 5(b)], and when using 22 OSVs the OSVMP2 based PES is already close to the curve of canonical MP2 (e.g., errors are around 0.05 and 0.3 mE_h for the stretched and contracted C–C bonds, respectively). In the case of dOSVMP2 and dOSVMP2-P with $N_v = 28$ OSVs, we see very tiny breaks (only 0.04 and 0.02 mE_h), respectively, at 1.559 and 1.597 Å. These discontinuities are, nevertheless, 1 order of magnitude smaller than those of the PAO $N_v = 34$ result discontinuities.

B. Virtual space size and timings

The efficiencies of both the Pulay-Saebø PAO and orbital-specific virtual approximations depend on the size of the virtual space needed to obtain good agreement with the canonical result. Figure 6 gives the comparison of virtual space sizes between PAO local MP2, dOSVMP2-P, and OSVMP2 needed to recover 99.99% of the correlation energy

(a)

(b)

FIG. 5. Potential energy surfaces (correlation energies) resulting from (a) Pulay-Saebø's PAO local MP2 [using MOLPRO (Ref. 37)] and (b) OSVMP2, dOSVMP2, and dOSVMP2-P for the central C=C bond of propadienone using a cc-pVDZ basis set (Ref. 50). The equilibrium geometry (Ref. 51) was obtained by optimizing all internal coordinates of propadienone at the MP2/cc-pVDZ level. The displacement of the central C=C bond was 0.001 Å and other internal coordinates were frozen. The insets magnify the details at the vicinity of the equilibrium C=C bonds (1.336 Å).
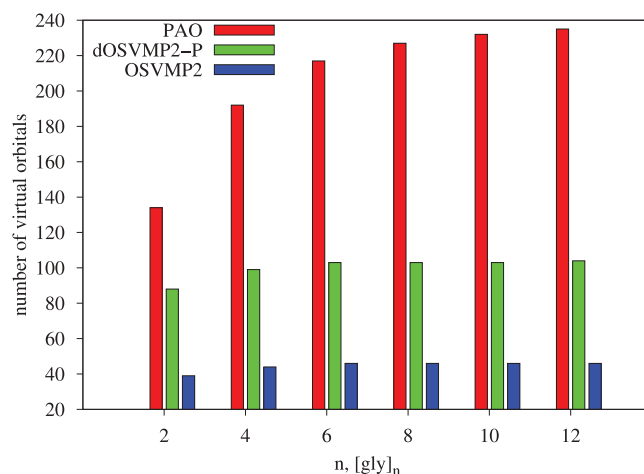

FIG. 6. Histograms of virtual orbital numbers for Pulay–Saebø's PAO local MP2, dOSVMP2-P, and OSVMP2 schemes needed to obtain 99.99% accuracy. In the case of PAO local MP2, this number is obtained from the average pair domain size.

TABLE V. CPU times (t_{solv}, s) to solve the dOSVMP2-P and OSVMP2 residual equations, using different screening thresholds T_S for [gly]$_n$ chains with $n = 4, 6, 8, 10, 12.103$ and 46 OSVs have been used respectively for dOSVMP2-P and OSVMP2 in order to obtain accuracies of 99.99% for all $T_S = 0.00$ computations. ΔE_{scrn} is the additional relative error in the correlation energy introduced by screening $T_S > 0.00$ as compared to $T_S = 0.00$. The cc-pVDZ basis set (Ref. 50) (denoted as D) was used for all computations and results with the cc-pVTZ basis set (denoted as T) are also reported for [gly]$_4$ and [gly]$_6$ molecules. With the cc-pVTZ basis set $N_v = 235$ ([gly]$_4$) and $N_v = 243$ ([gly]$_6$) were used for dOSVMP2-P while $N_v = 92$ ([gly]$_4$) and $N_v = 94$ ([gly]$_6$) were used for OSVMP2. Calculations were carried out on a 2.00 GHz 64-bit Intel Xeon CPU with 16 GB 667 MHz DDR2 RAM. The dual convergence criteria were set to 10^{-10} a.u. for residuals and 10^{-6} a.u. for correlation energies.

| | | | $N_v = 103$ for dOSVMP2-P | | | | | $N_v = 46$ for OSVMP2 | | | | |
| | PAO[a] | | $T_S = 0.00$ | $T_S = 0.20$ | | $T_S = 0.40$ | | $T_S = 0.00$ | $T_S = 0.07$ | | $T_S = 0.20$ | |
[gly]$_n$	t_{solv}[b]	t_{solv}[c]	t_{solv}[b]	t_{solv}[b]	ΔE_{scrn}(%)	t_{solv}[b]	ΔE_{scrn}(%)	t_{solv}[b]	t_{solv}[b]	ΔE_{scrn}(%)	t_{solv}[b]	ΔE_{scrn}(%)
4 (D)	417	401	470	378	0.0001	340	0.0002	625	307	0.0001	243	0.008
4 (T)	5311	4819	5375	4041	0.0001	3614	0.0001	4270	1692	0.0005	1415	0.010
6 (D)	1573	1281	1304	833	0.0001	749	0.0004	2104	742	0.0001	569	0.009
6 (T)	16150	12767	16429	10032	0.0002	8873	0.0004	13911	4015	0.0005	3328	0.010
8 (D)	3529	2437	2749	1466	0.0001	1310	0.0004	4739	1304	0.0001	985	0.010
10 (D)	7462	4038	5051	2284	0.0001	2027	0.0005	8982	2024	0.0001	1515	0.011
12 (D)	11621	5147	8249	3271	0.0001	2912	0.0005	15219	2901	0.0001	2154	0.011

[a]The averaged pair domain sizes are 192 (454 for T), 217 (520 for T), 227, 232, and 235, respectively, for $n = 4, 6, 8, 10, 12$.
[b]All internal occupied pairs are included.
[c]Distant and very distant pairs are discarded by default in MOLPRO with the settings rdist = 8 a.u. and rvdist = 15 a.u.

in [gly]$_n$. It is evident that PAO based local MP2 needs substantially more virtual orbitals (two times) than dOSVMP2-P and at least four times more than OSVMP2. Furthermore, the sizes of the orbital-specific virtual spaces for dOSVMP2-P and OSVMP2 saturate much more rapidly than those of PAO based MP2 when the molecular size increases. The relative advantage of the orbital-specific scheme increases as we move to the large basis. i.e.. from cc-pVDZ to cc-pVTZ.[50]

Tables V and VI give the central processing unit (CPU) times to solve the residual equations in the Pulay–Saebø PAO MP2, dOSVMP2-P, and OSVMP2 approaches for [gly]$_n$ chains and polyenes. In the case of PAO MP2, we report both the all-pair times (i.e., with no screening of distant pairs) as well as the times with the default MOLPRO screening thresholds. We consider the all-pair PAO MP2 times as the appropriate comparison, since the OSV approaches do not screen distant pairs. (Note that even when we employ a screening threshold T_S for the N^6 contraction as described in Sec. III E, the OSV methods are still working within an all-pair formalism).

We first discuss the results where $T_S = 0$. We find that the dOSVMP2-P times are generally comparable to or, in larger systems, faster than the PAO MP2 all-pair times (e.g., the $T_S = 0$ dOSVMP2-P calculation takes only 60% of the time of the PAO MP2 calculation in $C_{14}H_{16}$). The OSVMP2 times are longer than the PAO MP2 times in the case of the glycine chains but significantly shorter in the case of the polyenes.

The OSV methods' computational efficiency can be greatly improved by using the screening scheme discussed earlier. We have reinvestigated the CPU time of solving the residual equations using screening and the results are also presented in Tables V and VI. The threshold T_S is chosen such that there is only a very minor error in the correlation energy,

TABLE VI. CPU times (t_{solv}, s) to solve the dOSVMP2-P and OSVMP2 residual equations, using different screening thresholds T_S, for polyenes. The PAO computation recovers about 99.26% of the correlation energy. 100 and 40 OSVs have been used for dOSVMP2-P and OSVMP2, respectively. ΔE_{scrn} is the additional relative error of correlation energy introduced by screening $T_S > 0.00$ as compared to $T_S = 0.00$. For $T_S = 0.00$ the percentage (ΔE_{corr}) of the canonical MP2 energy recovered is also reported. The cc-pVTZ basis set was used for all computations. Calculations were carried out on a 2.00 GHz 64-bit Intel Xeon CPU with 16 GB 667 MHz DDR2 RAM. The dual convergence criteria were set to 10^{-10} a.u. for residuals and 10^{-6} a.u. for correlation energies.

| | | | $N_v = 100$ for dOSVMP2-P | | | | | | $N_v = 40$ for OSVMP2 | | | |
| | PAO[a] | | $T_S = 0.00$ | | $T_S = 0.10$ | | $T_S = 0.20$ | | $T_S = 0.00$ | | $T_S = 0.03$ | |
Polyenes	t_{solv}[b]	t_{solv}[c]	t_{solv}[b]	ΔE_{corr}(%)	t_{solv}[b]	ΔE_{scrn}(%)	t_{solv}[b]	ΔE_{scrn}(%)	t_{solv}[b]	ΔE_{corr}(%)	t_{solv}[b]	ΔE_{scrn}(%)
C_6H_8	21	20	26	99.61	24	0.001	23	0.004	15	99.54	11	0.002
C_8H_{10}	55	54	50	99.48	43	0.002	40	0.007	33	99.46	20	0.004
$C_{10}H_{12}$	115	110	86	99.39	69	0.003	63	0.009	63	99.41	32	0.005
$C_{12}H_{14}$	235	212	135	99.32	99	0.004	90	0.009	103	99.37	44	0.007
$C_{14}H_{16}$	383	314	224	99.27	137	0.004	123	0.009	164	99.34	62	0.008

[a]The averaged pair domain sizes are 140, 156, 167, 175, and 179, respectively, for each polyene.
[b]All internal occupied pairs are included.
[c]Distant and very distant pairs are discarded by default in MOLPRO with the settings rdist=8 a.u. and rvdist=15 a.u.

e.g., the screening errors are restricted to less than 0.01% of the correlation energy or only a few tenths of kilocalories per mole in the present study.

For the longest [gly]$_{12}$, dOSVMP2-P with $T_S = 0.20$ and OSVMP2 with $T_S = 0.07$ are, respectively, sped up by a factor of 2–3 and 5 compared to those with $T_S = 0.00$. As a result, both screened computations for [gly]$_n$ (with a screening error of $\Delta E_{scrn} = 0.0001\%$) are now almost two times faster than the Pulay–Saebø PAO even without accounting for the distant and very distant pairs. The screened cc-pVTZ results of dOSVMP2-P and OSVMP2 are shown for [gly]$_4$ and [gly]$_6$ in Table V. Clearly larger basis sets increase the efficiency of screened OSVMP2 computations relative to PAO and dOSVMP2-P. Polyene chains are more difficult cases, as the correlating orbitals are more extended along the chain than in [gly]$_n$. However, with a screening accuracy of $\Delta E_{corr} \leq 0.01\%$, we find that the screened dOSVMP2-P and OSVMP2 computations are still faster than the Pulay–Saebø implementation by a factor of 2 and 5, respectively.

VI. CONCLUSIONS

In this work we have described the direct orbital-specific and full orbital-specific virtual approximations to local second-order Møller–Plesset perturbation theory. These representations of the amplitudes have been expressed in a general language of tensor factorization that also encompasses many other representations used in electronic structure theory. As we have showed, the orbital-specific virtual approximation can lead to significant advantages, both in more formal behavior, such as smoothness of potential energy curves, as well as in practical times and accuracies, as compared to efficient implementations of the local Pulay–Saebø correlation ansatz. As for the direct versus full orbital-specific virtual approximations, when screening is used, the full orbital-specific virtual approximation is superior.

There is much to be done along the directions of this work. For example our algorithms are not linearly scaling for two reasons: first, we have not investigated efficient representations of the occupied space and second, an efficient integral transformation based on DF or RI is necessary for computing larger molecules. The relative advantages of the orbital-specific virtual approximation should also be compared numerically to pair natural orbital approaches, with which it shares some common features. The explicitly correlated effect such as R12/F12 corrections should be generalized to the orbital-specific virtual approximations. Finally, we expect that significant advantages can be had when applying orbital-specific virtual type approximations to high body excitations. We conclude by recognizing that the space of tensor factorizations is very large, with much remaining to be explored.

ACKNOWLEDGMENTS

[1]P. Pulay, Chem. Phys. Lett. **100** 151 (1983).
[2]P. Pulay and S. Saebø, Theor. Chim. Acta **69**, 357 (1986).
[3]S. Saebø and P. Pulay, J. Chem. Phys. **86**, 914 (1987).
[4]J. W. Boughton and P. Pulay, J. Comput. Chem. **14**, 736 (1993).
[5]C. Hampel and H. J. Werner, J. Chem. Phys. **104**, 6286 (1996).
[6]M. Schütz, G. Hetzer, and H. J. Werner, J. Chem. Phys. **111**, 5691 (1999).
[7]M. Schütz, Phys. Chem. Chem. Phys. **4**, 3941 (2002).
[8]M. Schütz and H. J. Werner, Chem. Phys. Lett. **318**, 370 (2000).
[9]M. Schütz and H. J. Werner, J. Chem. Phys. **114**, 661 (2001).
[10]W. Meyer, J. Chem. Phys. **58**, 1017 (1973).
[11]M. Head-Gordon, P. E. Maslen, and C. A. White, J. Chem. Phys. **108**, 616 (1998).
[12]C. Edmiston and M. Krauss, J. Chem. Phys. **42**, 1119 (1965).
[13]W. Meyer, Int. J. Quantum Chem. **S5**, 341 (1971).
[14]R. Ahlrichs, F. Driessler, H. Lischka, V. Staemmler, and W. Kutzelnigg, J. Chem. Phys. **62**, 1235 (1975).
[15]V. Staemmler and R. Jaquet, Theor. Chim. Acta **59**, 487 (1981).
[16]F. Neese, F. Wennmohs, and A. Hansen, J. Chem. Phys. **130**, 114108 (2009).
[17]F. Neese, A. Hansen, and D. G. Liakos, J. Chem. Phys. **131**, 064103 (2009).
[18]L. Adamowicz and R. J. Bartlett, J. Chem. Phys. **86**, 6314 (1987).
[19]L. Adamowicz, R. J. Bartlett, and A. J. Sadlej, J. Chem. Phys. **88**, 5749 (1988).
[20]T. L. Barr and E. R. Davidson, Phys. Rev. A **1**, 644 (1970).
[21]A. G. Taube and R. J. Bartlett, Collect. Czech. Chem. Commun. **70**, 837 (2005).
[22]A. G. Taube and R. J. Bartlett, J. Chem. Phys. **128**, 164101 (2008).
[23]A. Landau, K. Khistyaev, S. Dolgikh, and A. I. Krylov, J. Chem. Phys. **132**, 014109 (2010).
[24]A. E. Reed and F. Weinhold, J. Chem. Phys. **83**, 1736 (1985).
[25]R. A. Mata and H. J. Werner, Mol. Phys. **105**, 2753 (2007).
[26]J. L. Whitten, J. Chem. Phys. **58**, 4496 (1973).
[27]N. H. F. Beebe and J. Linderberg, Int. J. Quantum Chem. **7**, 683 (1977).
[28]D. W. O'neal and J. Simons, Int. J. Quantum Chem. **36**, 673 (1989).
[29]H. Koch, A. S. de Merás, and T. B. Pedersen, J. Chem. Phys. **118**, 9481 (2003).
[30]T. Kinoshita, O. Hino, and R. J. Bartlett, J. Chem. Phys. **119**, 7756 (2003).
[31]F. Aquilante, T. B. Pedersen, and R. Lindh, J. Chem. Phys. **126**, 194106 (2007).
[32]F. Aquilante and T. B. Pedersen, Chem. Phys. Lett. **449**, 354 (2007).
[33]F. Weigand, M. Kattannek, and R. Ahlrichs, J. Chem. Phys. **130**, 164106 (2009).
[34]T. S. Chwee and E. A. Carter, J. Chem. Phys. **132**, 074104 (2010).
[35]H. J. Werner, F. R. Manby, and P. J. Knowles, J. Chem. Phys. **118**, 8149 (2003).
[36]F. R. Manby, J. Chem. Phys. **119**, 4607 (2003).
[37]MOLPRO, a package of *ab initio* programs designed by H.-J. Werner and P. J. Knowles, version 2009.1, R. Lindh, F. R. Manby, M. Schütz, *et al.*, see http://www.molpro.net.
[38]S. R. White and R. L. Martin, J. Chem. Phys. **110**, 4127 (1999).
[39]J. Hachmann, W. Cardoen, and G. K. L. Chan, J. Chem. Phys. **125**, 144101 (2006).
[40]F. Mezzacapo, N. Schuch, M. Boninsegni, and J. I. Cirac, New J. Phys. **11**, 083026 (2009).
[41]H. J. Changlani, J. M. Kinder, C. J. Umrigar, and G. K. L. Chan, Phys. Rev. B **80**, 245116 (2009).
[42]S. Saebø and P. Pulay, Chem. Phys. Lett. **113**, 13 (1985).
[43]S. Saebø, W. Tong, and P. Pulay, J. Chem. Phys. **98**, 2170 (1993).
[44]G. Hetzer, P. Pulay, and H. J. Werner, Chem. Phys. Lett. **290**, 143 (1998).
[45]M. Schütz, G. Rauhut, and H. J. Werner, J. Phys. Chem. A **102**, 5997 (1998).

[46] E. A. Hylleraas, Z. Phys. **65**, 209 (1930).

[47] P. Pulay, S. Saebø, and W. Meyer, J. Chem. Phys. **81**, 1901 (1980).

[48] C. Angeli, K. L. Bal, and V. Bakken (2005), DALTON, a molecular electronic structure program, release 2.0, http://www.kjemi.uio.no/software/dalton/dalton.html.

[49] S. F. Boys, in *Quantum Theory of Atoms, Molecules and the Solid State*, edited by P. O. Löwdin (Academic, New York, 1966).

[50] T. H. Dunning, J. Phys. Chem. **90**, 1007 (1989).

[51] See supplementary material at http://dx.doi.org/10.1063/1.3528935 for relevant cartesian coordinates of studied molecules.

[52] J. T. Su, X. Xu, and W. A. Goddard III, J. Phys. Chem. A **108**, 10518 (2004).

[53] S. Grimme, M. Steinmetz, and M. Korth, J. Org. Chem. **72**, 2118 (2007).

[54] A. Schaefer, H. Horn, and R. Ahlrichs, J. Chem. Phys. **97**, 2571 (1992).

[55] A. Schaefer, C. Huber, and R. Ahlrichs, J. Chem. Phys. **100**, 5829 (1994).

[56] N. J. Russ and T. D. Crawford, J. Chem. Phys. **121**, 691 (2004).

[57] W. Klopper, F. R. Manby, S. Ten-no, and E. F. Valeev, Int. Rev. Phys. Chem. **25**, 427 (2006).

[58] H. J. Werner, J. Chem. Phys. **129**, 101103 (2008).

[59] T. B. Adler and H. J. Werner, J. Chem. Phys. **130**, 241101 (2009).

[60] J. E. Subotnik and M. Head-Gordon, J. Chem. Phys. **123**, 064108 (2005).